Mineral chemistry and geochronology of the potassic alkaline ultramafic Inagli complex, Aldan Shield, eastern Siberia

U. MUES-SCHUMACHER*, J. KELLER,

Min.-Pet. Institut, Alberstr. 23b, 79104 Freiburg, Germany

V. A. KONONOVA

IGEM, Staromonetny 35, 109017 Moscow, Russia

AND

P. J. SUDDABY

Dept. of Geology, Imperial College, Prince Consort Road, London SW7 2BP, UK

Abstract

The Inagli complex, one of several Mesozoic intrusive complexes of the Aldan Shield (Siberian Platform), exhibits a concentric structure comprising several alkaline ultramafic rock-types. A central dunite body is surrounded by olivine- and phlogopite-clinopyroxenites forming an inner rim. The outer rim consists of different shonkinitic and malignitic rocks. The K-Ar ages obtained for the whole complex vary around 132 Ma.

The dunites and clinopyroxenites are characterized by cumulate textures. With increasing modal abundances of clinopyroxene and subordinate phlogopite, the rocks develop to olivine-clinopyroxenite, shonkinite, and malignite with intercumulus potassium feldspar. Mineralogical characterization of the rocks suggests they evolved by fractional crystallization. The highly forsteritic olivines (Fo up to 95) require a melt as magnesian as mg# 87.1, representing ± 26 wt.% MgO. The parental melt is likely to be an olivine-, H_2O- and K_2O-rich picritic liquid of shoshonitic character. Major and trace element systematics show high *LILE/LREE* and *LREE/HFSE* ratios indicating the involvement of a subduction zone component in the genesis of these rocks.

KEYWORDS: Inagli intrusive complex, alkaline, ultramafic, high-MgO parent-melt, subduction zone component, Aldan Shield, Siberia.

Introduction

THE genesis of alkaline ultramafic complexes is still a matter of debate. This concerns the identification of the parent magmas and the characteristics of their mantle source regions (Eggler 1978; Wyllie, 1978; Edgar, 1987), as well as subsequent fractionation processes during ascent. Uncertainties chiefly concern the compositions of these melts, notably their alkali content and oxidation state. In this respect, the Inagli complex is suitable for petrological studies because it displays a wide range of lithologies generated from an alkaline ultrabasic parent magma by fractionation processes.

An extensive drilling programme and prospecting by test pits was carried out at Inagli for platinum exploration. Providing fresh dunite samples, the deepest drill hole reached a depth of 900 m. The

* Present address: Hauptstr. 3, D-71672, Marbach, Germany

association of platinum-group minerals and chromitite in ultramafic intrusions has recieved much attention in recent years. Such an association is known in ophiolites, alpine-type peridotites, Alaskan complexes and stratiform intrusions (Peck and Keays, 1990).

In this paper we present petrographic, mineral and chemical data for a suite of ultramafic rocks. The scope is to give an idea of the petrogenesis and evolution of the ultramafic rocks with particular attention to the composition of the parent magma and the mantle source components involved.

Regional geological setting

The Inagli complex, a zoned ultramafic alkaline intrusion in the Archaean granulitic basement of the Aldan Shield, is exposed over an area of approximately 20 km^2 (Fig. 1). The Aldan Shield itself forms the southeastern part of the Siberian platform, and consists of Archaean to Proterozoic granulites and granites with intercalated metabasites (Bilanenko *et al.*, 1984; Perchuk *et al.*, 1985). It is subdivided by major WSW−ENE striking Mesozoic structures which are, south to north: (1) the Stanovoy zone with Jurassic granitic batholiths; (2) a Mesozoic depression zone with coal deposits; (3) the Aldan Uplift zone with Cambrian sediments overlain by the Lower Jurassic; and (4) the Aldan Anticline where the Precambrian basement dips at a low angle under the sedimentary cover of the Siberian platform (Kostyuk, 1983; Bilanenko *et al.*, 1984; Perchuk *et al.*, 1985). Magmatic activity is recognized throughout the entire geologic evolution of the Aldan Shield. Five periods of alkaline magmatism can be identified: (1) Palaeoproterozoic; (2) Neoproterozoic; (3) Devonian; (4) Mesozoic; and (5) Cenozoic (Bilibin, 1961, Maksimov, 1972).

The Inagli complex is one of the Mesozoic alkaline complexes of the Aldan Uplift zone (Kortschagin, 1972, 1986) and it comprises mainly ultramafic rocks (Fig. 1*b*). The central dunite body of approximately 4.5 km in diameter is surrounded concentrically by different types of clinopyroxenites which in turn are surrounded by shonkinites and malignitic rocks ('shonkinites' in Fig. 1*b* after Kortschagin, 1986). These outer concentric zones are 1.5 km wide. The central dunite is threaded by numerous pegmatitic veins and veinlets of diverse mineral assemblages which include phlogopite, potassium feldspar, chromium diopside, richterite and Mg-arfvedsonite (Kortschagin, 1986). Inagli intrudes widespread syenite porphyries which are of Upper Jurassic age (150 Ma, Kortschagin, 1986; 180 Ma, Pervov, pers. comm.). They are distinctly older than Inagli for which Kostyuk *et al.* (1990) determined an age of 129 ± 15 and 136 ± 5 Ma and this study 132 Ma. It is,

therefore, questionable whether the syenite porphyries are gentically related to Inagli.

Analytical methods

Modal component analyses were obtained by counting at least 3000 points on thin sections. Mineral chemistry was obtained by microprobe (WDS) and electron microscope (EDX) analyses. EDX analyses were performed at Freiburg with a Cambridge S4-10 scanning electron microscope with a KEVEX 7000 energy dispersive system. The analytical conditions were 15 kV accelerating voltage, 1 nA beam current, scanned over a 10 × 10 μm area, for 100 s dead-time corrected. WDS analyses were carried out at the Institute of Archaeometallurgy in Bochum with a Jeol 6400.

Some of the Inagli rocks have been dated by the conventional K-Ar method. Determinations of isotopic compositions were performed on two grain-size fractions of mineral separates and whole rock. The K-Ar analyses as well as the Rb-Sr analyses were carried out in the isotope laboratory of the University in Berne (extended methodical descriptions in Flisch, 1986; Hurford *et al.*, 1986). Sample ages were calculated using the constants of Steiger and Jäger (1977).

One sample has been analysed for Rb-Sr isotopes. Dissolved Rb and Sr samples were mixed with highly enriched ^{84}Sr and ^{87}Rb spikes, respectively. Rb and Sr were separated from each other with cation exchange columns and the isotopes were measured by the isotope dilution method. Rubidium isotope determinations were carried out on an 'Ion Instruments' mass spectrometer with 35 cm radius and a three filament ion source; Sr analyses were carried out on a VG sector mass spectrometer with 26 cm radius with one filament ion source and a five cup system (Hurford *et al.*, 1986). The precision of the ^{87}Sr/^{86}Sr ratio is better than 0.015%. NBS 987 was analysed as a standard for Sr analyses.

The ultramafic Inagli intrusion

The ultramafic Inagli intrusion consists of a dunite-clinopyroxenite-shonkinite-malignite series with dunite dominant (Fig. 1*b*). These rocks are generally massive and medium grained but coarse-grained variants also occur. All of the rock types may be chromite/magnetite- and/or phlogopite-bearing. With increasing amounts of clinopyroxene, feldspar, and feldspathoids the rocks grade into clinopyroxenite, shonkinite, and malignite. The salic minerals are potassium feldspar, (pseudo)leucite, nepheline/potassium feldspar-intergrowns, and sodalite.

Dunite. Dunites are formed by medium to coarse grained high Mg-olivines (Fo$_{89-95}$) with cumulate
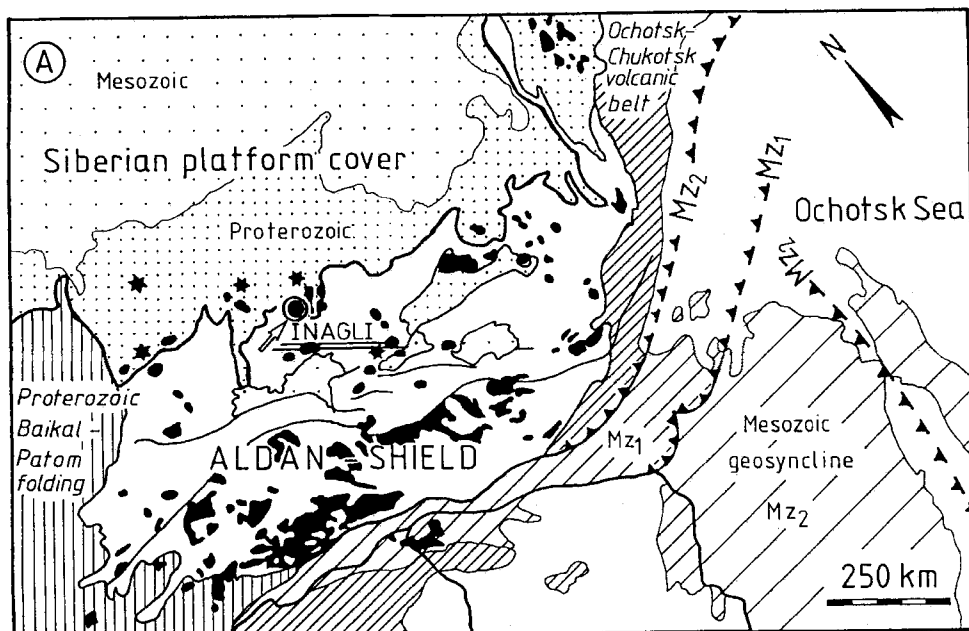
Legend for A and C

☐ ALDAN - SHIELD
✱ Mesozoic lamproites
◆ Mesozoic intrusions
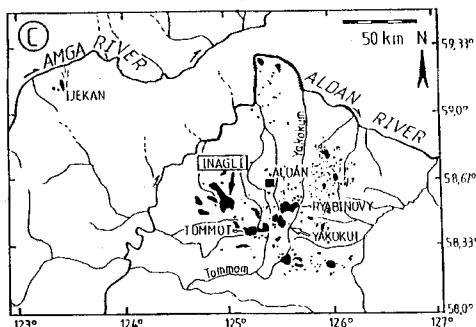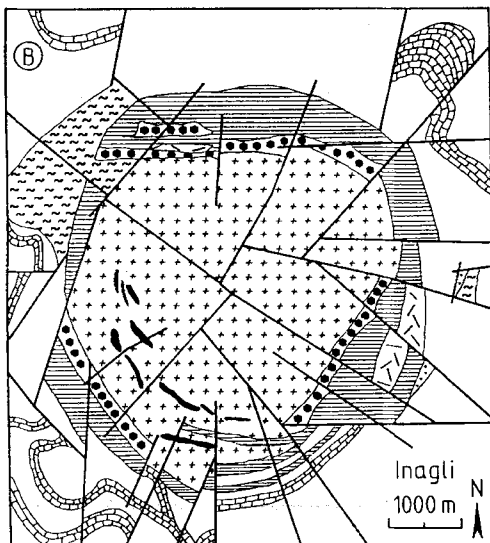
Legend for B

Dunite
Cr-Diopside Pegmatite
Phlog - Pyroxenite
Shonkinite
Pulaskite
Syenite Porphyry
Dolomite
Sandstone
Gneiss, Migmatite

FIG. 1. Sketch map of the Aldan Shield (A) and the concentric formed alkaline ultramafic Inagli complex (B) after Kortschagin, 1986. The inset (C) shows the Aldan area and, in black, the distribution of Mesozoic alkaline complexes after Bilibin, 1961. The bold boundary in (A) marks the boundary between the Aldan Shield and the Proterozoic sedimentary cover of the Siberian platform. Mz_1 (Early Mesozoic) and Mz_2 (Late Mesozoic) indicate the seismicity reflection zones.

TABLE 1. Modal composition in vol.% of the rocks of the Inagli complex with classification of the rocks after LeBas *et al.* (1986) and LeMaitre *et al.* (1989). Results obtained by point-counting at least 3000 points per sample

(a)	ol	cpx	phlog	spi	apa	leuc
Dunite						
AIN 4	97.2	–	1.7	1.0	–	–
AIN 9	98.3	–	–	1.7	–	–
AIN 30b	97.6	–	–	2.3	–	–
olivine-clinopyroxenite						
AIN 17	32.4	58.3	2.3	0.2	1.0	5.5
AIN 42	34.3	54.8	2.7	0.5	0.9	6.6
AIN 66	21.1	68.4	2.3	3.5	1.1	3.4
AIN 67	21.3	65.1	3.1	4.0	2.2	4.2
Phlogopite-clinopyroxenite						
AIN 13	1.2	58.9	27.8	1.4	10.4	–
AIN 14	0.5	77.6	12.8	2.9	6.1	–
AIN 34	1.0	57.0	30.6	1.4	9.9	–
AIN 63	6.2	54.0	28.3	2.0	6.1	3.2
AIN 64	7.8	63.0	23.5	0.1	4.9	0.4

(b)	ol	cpx	bio	spi	apa	leuc
Shonkinite						
AIN 16	20.8	46.8	2.2	1.1	1.7	27.2
AIN 25	24.1	48.5	1.2	0.6	1.6	23.8
AIN 62	9.1	62.1	2.8	5.7	4.1	15.9
Malignite						
olivine-rich						
AIN 39	16.9	33.2	1.4	1.8	2.0	44.7
AIN 40	14.8	40.8	1.3	0.8	2.7	39.4
AIN 43	13.5	32.8	2.5	2.2	3.2	45.5
AIN 44	18.8	38.4	4.4	1.3	2.8	34.2
olivine-poor						
AIN 15	–	25.4	14.9	3.0	1.7	54.7
AIN 23	1.9	28.0	6.0	3.4	1.8	58.6
AIN 24	4.7	35.5	4.9	3.8	2.4	48.5
AIN 26	3.6	28.5	2.2	3.9	1.6	59.9
AIN 50	–	34.4	17.5	2.0	2.1	43.9
AIN 58	2.3	24.1	5.7	5.3	1.3	61.1
AIN 59	1.8	29.8	4.6	3.8	1.7	58.1
AIN 61	–	38.3	11.5	–	2.1	47.9

Abbreviations: ol – olivine; cpx – clinopyroxene; phlog – phlogopite; bio – biotite; spi – spinel; apa – apatite; and leuc – leucocratics (Potassium feldspar and feldspathoids). (a) for the ultramafic rocks, (b) for shonkinites and malignites

fabric. The rocks additionally contain chromite and phlogopite (Fig. 2a; Table 1a). Olivine is generally fresh except for local slight serpentinization at grain boundaries and individual grains exhibit strain lamellae. The CaO contents are as high as 0.1–0.5 wt.% and NiO varies from 0.05 to 0.26 wt.% (Fig. 3a; Table 2). At contacts with veins or veinlets, individual olivines are up to 4 mm in size. They have no chromite inclusions, and show strain lamellae. Alignments of small granoblastic olivines
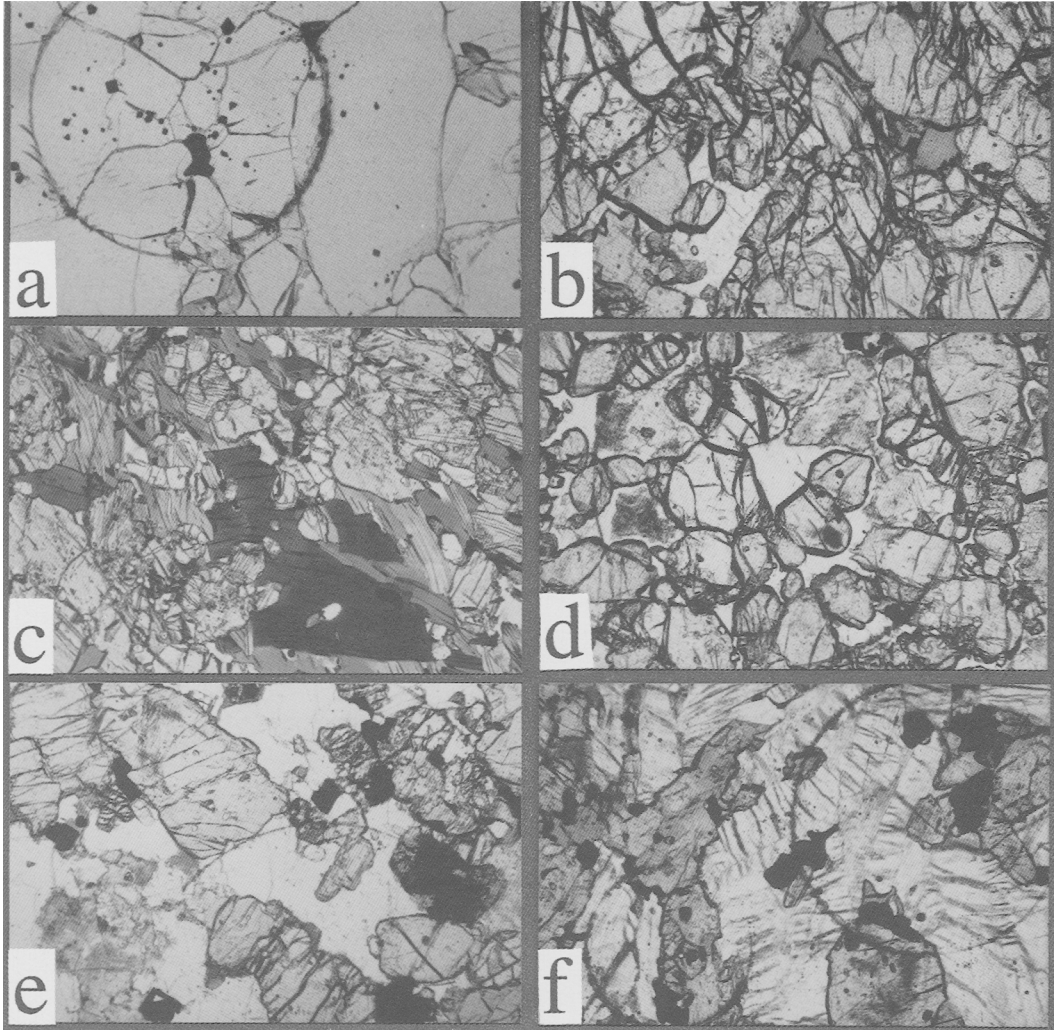
FIG. 2. Characteristic appearance of the different ultramafic, shonkinitic and malignitic rocks in thin section. All fields of view are approximately 1.6 mm wide. (a) Dunite: Small chromites between olivine. (b) Olivine-clinopyroxenite: Interstitial phlogopite and potassium feldspar within the dominating clinopyroxene and olivine. (c) Phlogopite-clinopyroxenite: Clinopyroxenes are often mantled by phlogopite and euhedral apatites are quite abundant. (d) Shonkinite: In between early clinopyroxenes and olivines, potassium feldspar crystallized. (e) Olivine-rich malignite: The mafic minerals occur as glomerophyric patches within potassium feldspar and minor leucite. (f) Olivine-poor malignite: The mafics (clinopyroxene and minor magnetite) occur in a 'groundmass' of potssium feldspar.

without strain lamellae occur on grain boundaries of larger olivines. Large chromites, often mantled by phlogopite, are abundant within these alignments of small olivine grains (Fig. 2a).

Chromites are generally Fe^{3+}-rich Ti-Al-magnesiochromites (0.57–1.65 wt.% TiO_2, 3.7–8.5 wt.% Al_2O_3, 6.1–15.7 wt.% MgO; Table 3) with Cr/ (Cr+Al) ratios of 0.84 to 0.99 and $Mg/(Mg+Fe^{2+})$ varying between 0.3 and 0.7 (Fig. 3b). Interstitial phlogopites are zoned with cores having high TiO_2 (0.5–2 wt.%), high Al_2O_3 (7–14 wt.%), and low FeO (4–7 wt.%) relative to the rims with lower TiO_2 (<0.4 wt.%), low Al_2O_3 (<2 wt.%; Fig. 3f), and higher Fe) (>17 wt.%; Table 4). The rims show reversed
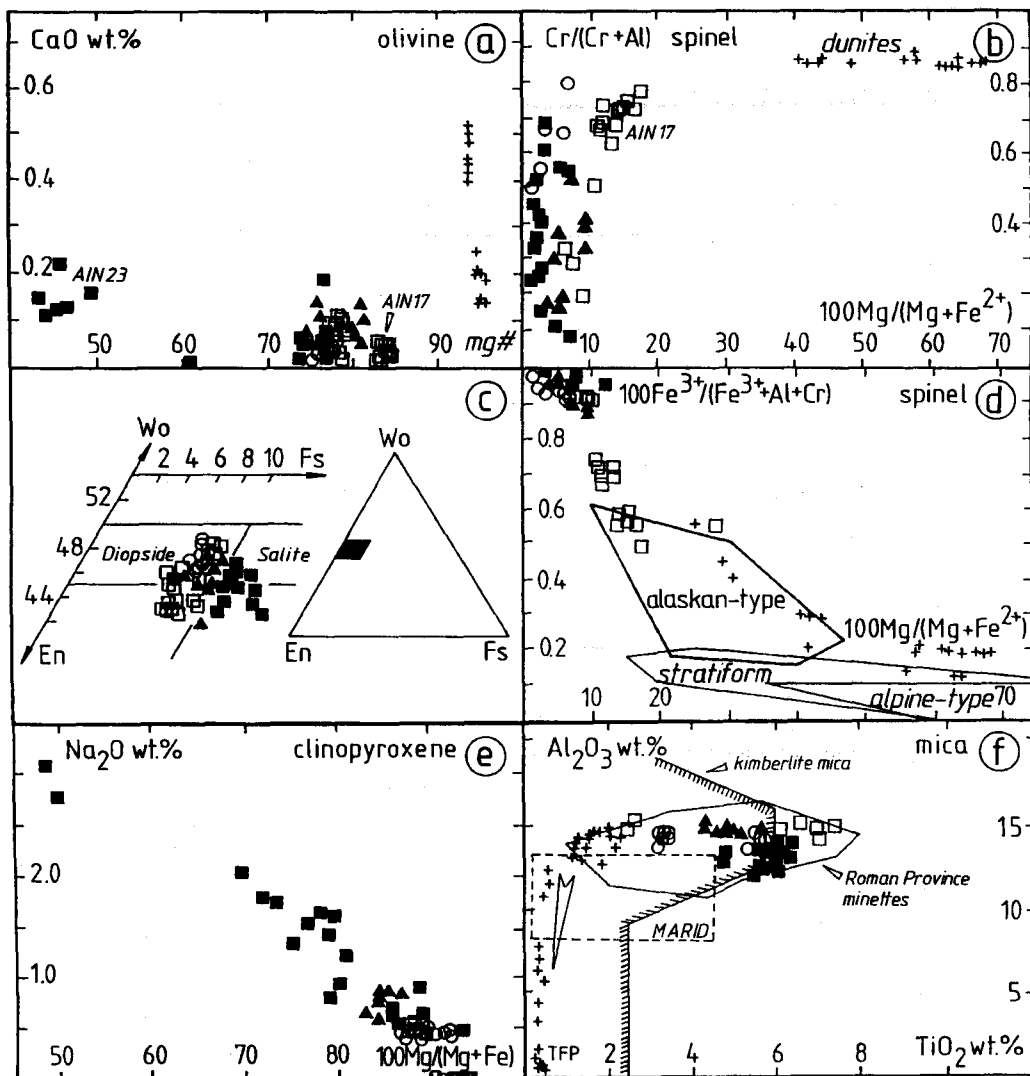
FIG. 3. Variation diagrams for mineral compositions. Symbols: +, dunites; □, olivine-clinopyroxenites; ○, phlogopite-clinopyroxenites; ▲, shonkinites; ■, malignites. (*a*) CaO *vs.* Mg# of olivines from the Inagli rocks. Mg# = 100Mg/(Mg+Fe). (*b*) 100Cr/(Cr+Al) *vs.* 100Mg/(Mg+Fe^{2+}) ratios of spinels showing their evolutionary trend for the rocks. (*c*) Wo-En-Fs-diagram for clinopyroxenes. Most pyroxenes are diopsides with salite compositions of olivine-poor malignites. (*d*) 100Mg/(Mg+Fe^{2+}) *vs.* 100Fe^{3+}/Fe^{3+}+Al+Cr for spinels. Fields for alpine-type peridotites, stratiform intrusions and Alaskan-type plutonic complexes are adapted from Irvine (1967). (*e*) Na$_2$O *vs.* 100Mg/(Mg+Fe) for clinopyroxenes, showing a Na$_2$O enrichment trend which is due to an acmite component in clinopyroxenes from the olivine-poor malignites. (*f*) Al$_2$O$_3$ *vs.* TiO$_2$ variation diagram for mica from the Inagli complex. For comparison, the fields for MARID, kimberlite mica and Roman Province minettes are shown (Mitchell and Bergman, 1991). Most of the mica from Inagli match the field of Roman Province minettes. Phlogopite rims of the dunites are Al$_2$O$_3$- and TiO$_2$-poor showing tetraferriphlogopitic (TFP) compositions.

pleochroism and are of tetraferriphlogopitic composi-
tions with Si + Al + Ti < 8.

Clinopyroxenite. The cumulitic textured clino-
pyroxenites contain 54–78 vol.% subhedral, colour-

TABLE 2. Wavelength-dispersive microprobe analyses of olivine from the Inagli rocks. Each analysis represents the average of several individual olivine compositions with 1σ standard deviations (n – number of analyses)

	AIN 4 (n=8) dunite	AIN 9 (n=7) dunite	AIN 17 (n=17) ol-pyroxenite	AIN 67 (n=9) ol-pyroxenite	AIN 63 (n=3) phlog-pyrox.	AIN 64 (n=6) phlog-pyrox.
SiO_2	39.32 ± 0.57	40.40 ± 1.50	40.02 ± 0.75	39.72 ± 0.69	38.78 ± 0.37	38.34 ± 0.50
Cr_2O_3	0.02 ± 0.04	0.03 ± 0.02	n.a.	n.a.	n.a.	n.a.
FeO	5.02 ± 0.37	6.35 ± 0.17	15.52 ± 0.54	19.35 ± 0.59	20.45 ± 0.14	21.34 ± 0.93
MnO	n.a.	n.a.	n.a.	n.a.	0.43 ± 0.03	0.48 ± 0.05
NiO	0.29 ± 0.03	0.24 ± 0.04	0.11 ± 0.03	0.10 ± 0.04	0.11 ± 0.03	0.12 ± 0.04
MgO	55.18 ± 0.57	52.52 ± 1.34	44.29 ± 0.39	40.32 ± 0.41	40.19 ± 0.26	39.63 ± 0.58
CaO	0.18 ± 0.03	0.45 ± 0.04	0.06 ± 0.10	0.07 ± 0.03	0.04 ± 0.01	0.05 ± 0.03
Total	100.01 ± 1.61	99.99 ± 3.11	100.00 ± 1.81	100.00 ± 1.81	100.00 ± 0.84	99.96 ± 2.13
Mg#	0.951 ± 0.003	0.936 ± 0.001	0.836 ± 0.004	0.788 ± 0.006	0.778 ± 0.001	0.768 ± 0.010

	AIN 16 (n=3) shonkinite	AIN 25 (n=3) shonkinite	AIN 62 (n=4) shonkinite	AIN 44 (n=8) malignite	AIN 58 (n=3) malignite	58 (1) malignite	AIN 23 (n=6) malignite
SiO_2	40.07 ± 0.87	39.98 ± 0.34	38.78 ± 0.49	38.41 ± 0.54	37.43 ± 0.19	29.57	34.44 ± 0.45
Cr_2O_3	n.a.	n.a.	n.a.	0.01 ± 0.03	n.a.	n.a.	0.03 ± 0.02
FeO	18.45 ± 0.68	17.65 ± 0.22	22.13 ± 0.51	21.24 ± 0.31	23.62 ± 0.11	37.21	44.52 ± 1.12
MnO	0.41 ± 0.03	0.37 ± 0.00	0.58 ± 0.04	0.51 ± 0.02	0.94 ± 0.05	0.90	n.a.
NiO	0.13 ± 0.02	0.10 ± 0.03	0.08 ± 0.04	0.13 ± 0.03	0.08 ± 0.04	0.07	n.a.
MgO	40.87 ± 0.16	42.80 ± 0.17	38.36 ± 0.57	39.62 ± 0.45	37.88 ± 0.20	32.24	20.87 ± 1.16
CaO	0.07 ± 0.01	0.09 ± 0.03	0.09 ± 0.03	0.07 ± 0.05	0.04 ± 0.02	0.01	0.14 ± 0.03
Total	100.00 ± 1.77	99.99 ± 0.79	100.02 ± 1.68	100.00 ± 0.84	99.99 ± 0.61	100.00	100.00 ± 2.78
Mg#	0.798 ± 0.005	0.812 ± 0.002	0.755 ± 0.006	0.769 ± 0.003	0.741 ± 0.001	0.607	0.455 ± 0.019

n.a. - not analysed

Table 3. Representative wavelength-dispersive electron microprobe analyses of spinels from the Inagli rocks

Sample	4−11 dunite	4−17 dunite	9−9 dunite	9−11 dunite	17−4 olcpx	17−37 olcpx	67−8 olcpx	63−4 phlcpx
TiO_2	0.57	0.92	0.75	0.78	2.47	3.63	5.99	0.35
Al_2O_3	4.99	6.88	5.72	5.06	5.90	4.36	2.50	0.02
Cr_2O_3	60.09	56.68	50.13	50.66	30.21	12.49	1.48	0.03
FeO_{tot}	22.55	22.55	32.19	32.51	53.62	68.27	78.16	88.75
MnO	0.38	0.35	0.52	0.55	0.59	0.42	0.35	0.06
MgO	11.63	12.95	9.52	8.50	3.38	2.15	1.56	0.22
Total	100.21	100.33	98.83	98.06	96.17	91.32	90.04	89.43
Recalculated analyses								
Fe_2O_3	7.94	9.40	15.27	14.30	28.12	42.56	50.69	65.65
FeO	15.40	14.09	18.45	19.64	28.31	29.96	32.54	29.66
Total	101.00	101.27	100.36	99.49	98.98	95.57	95.10	95.99
Mol.% end member spinel molecules								
$MgAl_2O_4$	9.8	13.2	11.4	10.3	12.6	9.9	5.8	0.0
Mg_2TiO_4	1.4	2.3	1.9	2.0	2.8	1.2	1.7	0.6
Mn_2TiO_4	−	−	−	−	0.9	0.7	0.6	0.1
Fe_2TiO_4	−	−	−	−	2.1	7.9	14.8	0.2
$MnCr_2O_4$	1.1	1.0	1.5	1.6	—	—	—	—
$MgCr_2O_4$	45.0	45.2	32.9	29.4	—	—	—	—
$FeCr_2O_4$	32.9	26.9	32.8	38.1	43.3	18.9	2.3	0.0
Fe_3O_4	9.9	11.5	19.5	18.6	38.3	61.4	74.8	99.0
Structural formula based on 32 oxygens								
Ti	0.105	0.169	0.141	0.148	0.479	0.835	1.306	0.084
Al	0.722	0.990	0.845	0.752	0.897	0.786	0.427	0.004
Cr	5.832	5.473	4.967	5.048	3.081	1.510	0.170	0.004
Fe^{3+}	1.543	1.535	2.249	2.284	3.857	4.897	6.317	7.913
Fe^{2+}	3.163	2.878	3.867	4.140	6.108	7.662	7.888	7.947
Mn	0.079	0.072	0.110	0.117	0.129	0.109	0.086	0.016
Mg	4.256	4.715	3.557	3.194	1.300	0.980	0.674	0.105
Total	15.700	15.833	15.736	15.683	15.851	16.779	16.867	16.074
Cr#	0.890	0.847	0.855	0.870	0.775	0.658	0.284	0.502

olcpx − olivine-clinopyroxenite; phlcpx − phlogopite-clinopyroxenite; shonk − shonkinite; malig − malignite; $cr\# = Cr/(Cr+Al)$

less or pale green clinopyroxene up to 1.5 mm in size (Table 1*a*; Fig. 2*b*). Zoning is rare, and analyses vary chiefly between $Ca_{42}Mg_{43}Fe_7$ and $Ca_{49}Mg_{50}Fe_9$ (Table 5). All of the clinopyroxenites may be olivine- and phlogopite-bearing with olivine surrounding pyroxenes. In some variants, termed olivine-clino-pyroxenites, olivine is a major component (20–35 vol.%) with only minor phlogopite (up to 2.5%, Table 1*a*). Rocks with higher amounts of phlogopite (12–31 vol.%) and less than 8 vol.% olivine are termed phlogopite-clinopyroxenites (Table 1*a*).

In olivine-clinopyroxenites, olivine (Fo_{75-84}) is mostly fresh, and larger crystals intimate strain lamellae. In contrast, olivine is almost entirely altered to iddingsite in phlogopite clinopyroxenites. The CaO contents of all olivines are very low (<0.1%) while NiO varies within 0.05–0.18% (Table 2). Spinels in olivine-clinopyroxenites are mostly chromites (TiO_2 <4 wt.%, Al_2O_3 <6.6 wt.%, MgO <3.5 wt.%) with only minor Ti-bearing magnetites (up to 7.6 wt.% TiO_2; Table 3). Phlogopite mantles pyroxene, olivine, and euhedral

TABLE 3 (*cont.*) Spinel analyses

sample	64−24 phlcpx	16−5 shonk	62−12 shonk	62−18 shonk	23−9 malig	23−12 malig	44−17 malig	58−5 malig
TiO_2	2.97	4.90	4.69	7.41	11.48	12.43	1.24	7.83
Al_2O_3	1.14	3.00	1.52	1.42	0.27	0.14	0.57	0.85
Cr_2O_3	3.24	2.14	0.48	0.41	0.14	0.17	1.83	0.11
FeO_{tot}	85.32	81.55	85.86	82.52	81.17	81.54	85.40	80.40
MnO	0.28	0.45	0.29	0.43	0.76	0.63	0.23	0.64
MgO	1.10	1.86	0.78	1.16	0.69	0.44	0.57	1.55
Total	94.05	93.90	93.62	93.35	94.51	95.35	89.84	91.38
Recalculated analyses								
Fe_2O_3	59.40	54.71	57.87	52.56	46.70	45.24	61.78	51.66
FeO	31.86	32.31	33.77	35.21	39.13	40.82	29.79	33.90
Total	99.98	99.37	99.40	98.60	99.18	99.87	96.01	96.54
Mol.% end member spinel molecules								
$MgAl_2O_4$	2.5	6.6	3.4	3.2	0.6	0.3	1.3	2.0
Mg_2TiO_4	1.8	1.9	0.5	1.7	1.7	1.1	1.0	3.5
Mn_2TiO_4	0.4	0.7	0.5	0.7	1.2	1.0	0.4	1.1
Fe_2TiO_4	5.7	10.5	12.0	18.2	28.9	32.5	1.9	17.4
$MgCr_2O_4$	−	−	−	−	−	−	−	−
$FeCr_2O_4$	4.8	3.2	0.7	0.6	0.2	0.3	2.9	0.2
Fe_3O_4	84.6	77.1	82.9	75.6	67.3	64.8	92.5	75.9
Structural formula based on 32 oxygens								
Ti	0.649	1.102	1.010	1.554	2.299	2.834	0.291	1.685
Al	0.195	0.528	0.257	0.233	0.042	0.025	0.105	0.143
Cr	0.372	0.253	0.054	0.045	0.015	0.020	0.226	0.012
Fe^{3+}	6.907	6.147	6.852	6.419	6.024	5.162	7.438	6.412
Fe^{2+}	7.736	8.071	8.085	8.214	8.713	10.350	7.784	8.111
Mn	0.069	0.115	0.071	0.102	0.171	0.162	0.061	0.155
Mg	0.476	0.827	0.334	0.483	0.274	0.199	0.265	0.661
Total	16.404	17.042	16.663	17.052	17.537	18.752	16.171	17.180
Cr#	0.656	0.324	0.175	0.163	0.258	0.449	0.683	0.080

Abbreviations as on previous page

spinel. They are commonly unzoned with a relatively wide and unsystematic variation in their TiO_2 contents (3−7.5 wt.%; Table 4). Apatite occurs as an accessory phase (<2.5 %) in olivine-clinopyroxenites, while it becomes more important in phlogopite-clinopyroxenites which have up to 10.5 vol.% apatite (Table 1a). The latter include apatite either as euhedral inclusions in pyroxene and phlogopite or as fine-grained aggregates in larger interstices. In the olivine-clinopyroxenites, potassium feldspar occupies intersticies with 3.5−6.5 vol.%.

Cumulate phases of all clinopyroxenites are pyroxene and olivine with intercumulus potassium feldspar, phlogopite, and apatite. In the phlogopite-clinopyroxenites, phlogopite and apatite occur both as additional cumulate phases as well as within the intercumulus assemblage.

Shonkinite. The shonkinites show a clear mesocumulitic texture. Cumulus phases are minor olivines ($Fo_{74−83}$) with CaO and NiO <0.15 wt.% (Table 2) and prevalent euhedral, colourless to pale green clinopyroxenes (Fig. 2d, Table 1b). Clinopyroxenes have abundant spinel and apatite inclusions, and analyses vary between $Ca_{42}Mg_{44}Fe_7$ and $Ca_{46}Mg_{47}Fe_{11}$ with relatively high Na_2O contents (0.5−1.0 wt.%, Table 5). Accessory phases are

TABLE 4. Average energy-dispersive electron microscope analyses with 1σ errors of phlogopites from the Inagli rocks. For the phlogopites of the dunites averages of c – cores and r – rims are given

	AIN 2-c (8) dunite	AIN 2-r (8) dunite	AIN 4-c (7) dunite	AIN 4-r (7) dunite	AIN 67 (7) ol-pyroxenite	AIN 34 (10) phlog-pyroxe.
SiO_2	41.82 ± 0.53	41.40 ± 0.44	41.02 ± 0.26	42.05 ± 0.61	38.63 ± 0.48	39.38 ± 0.33
TiO_2	0.62 ± 0.35	0.27 ± 0.05	1.61 ± 0.20	0.30 ± 0.03	5.42 ± 1.86	3.13 ± 0.10
Al_2O_3	10.24 ± 2.26	1.23 ± 1.62	13.71 ± 0.58	4.91 ± 2.12	14.22 ± 0.22	13.56 ± 0.16
Cr_2O_3	0.20 ± 0.18	0.00 ± 0.00	1.34 ± 0.23	0.00 ± 0.00	0.00 ± 0.00	0.00 ± 0.00
FeO	6.65 ± 2.01	16.90 ± 2.04	2.74 ± 0.67	11.54 ± 2.71	9.09 ± 1.06	10.21 ± 0.49
MgO	26.63 ± 0.51	26.75 ± 0.17	25.66 ± 0.24	27.17 ± 0.27	19.30 ± 0.71	20.02 ± 0.33
K_2O	9.83 ± 0.09	9.46 ± 0.22	9.92 ± 0.10	9.81 ± 0.17	9.31 ± 0.16	9.69 ± 0.14
Total	95.99 ± 5.93	96.01 ± 4.54	96.00 ± 2.28	95.78 ± 5.91	95.97 ± 4.49	95.99 ± 1.55

	AIN 63 (10) phlog-pyroxe.	AIN 16 (8) shonkinite	AIN 26 (6) malignite	AIN 39 (3) malignite	AIN 43 (9) malignite
SiO_2	39.20 ± 0.26	39.04 ± 0.40	39.16 ± 0.31	38.74 ± 0.25	38.97 ± 0.12
TiO_2	5.51 ± 0.21	4.60 ± 0.39	5.54 ± 0.20	5.41 ± 0.18	5.70 ± 0.54
Al_2O_3	13.33 ± 0.20	14.13 ± 0.22	11.97 ± 0.11	13.46 ± 0.31	13.34 ± 0.23
Cr_2O_3	0.00 ± 0.00	0.00 ± 0.00	0.00 ± 0.00	0.00 ± 0.00	0.00 ± 0.00
FeO	7.89 ± 0.65	8.10 ± 0.26	11.51 ± 0.50	8.48 ± 0.38	9.07 ± 0.40
MgO	20.72 ± 0.51	20.14 ± 0.43	17.81 ± 0.41	19.62 ± 0.25	18.84 ± 0.54
Na_2O	0.33 ± 0.17	0.11 ± 0.15	0.16 ± 0.16	0.33 ± 9.96	0.00 ± 0.00
K_2O	9.03 ± 0.15	9.86 ± 0.15	9.86 ± 0.05	9.96 ± 0.20	10.07 ± 0.12
Total	96.01 ± 2.15	95.98 ± 2.00	96.01 ± 1.74	96.00 ± 1.86	95.99 ± 1.95

TABLE 5. Wavelength-dispersive microprobe analyses of clinopyroxenes from the Inagli rocks. Each analysis represents the average of several individual clinopyroxene compositions with standard deviations (n – number of analyses). Fe_2O_3 contents are calculated from acmite component

	AIN 17 (10) ol-pyroxenite	AIN 67 (7) ol-pyroxenite	AIN 63 (6) phlog-pyrox.	AIN 64 (11) phlog-pyrox.	AIN 16 (4) shonkinite	AIN 62 (4) shonkinite
SiO_2	54.56 ± 0.76	52.44 ± 0.75	53.40 ± 0.46	53.12 ± 0.86	53.56 ± 0.42	53.80 ± 0.80
TiO_2	0.37 ± 0.07	0.46 ± 0.08	0.31 ± 0.11	0.26 ± 0.08	0.44 ± 0.11	0.49 ± 0.06
Al_2O_3	1.63 ± 0.17	1.24 ± 0.04	0.73 ± 0.14	0.97 ± 0.14	2.40 ± 0.67	1.21 ± 0.16
Cr_2O_3	0.30 ± 0.15	0.03 ± 0.04	0.06 ± 0.05	0.07 ± 0.07	0.30 ± 0.26	0.04 ± 0.05
Fe_2O_3	0.00 ± 0.00	2.53 ± 0.02	2.63 ± 0.03	2.27 ± 0.03	3.09 ± 0.15	3.92 ± 0.11
FeO	4.84 ± 0.23	4.08 ± 0.17	3.18 ± 0.17	3.16 ± 0.26	2.58 ± 0.69	2.43 ± 0.15
MgO	17.04 ± 0.37	15.91 ± 0.12	16.12 ± 0.17	16.18 ± 0.20	16.06 ± 0.28	15.59 ± 0.23
CaO	21.25 ± 0.56	24.04 ± 0.59	23.33 ± 0.20	23.75 ± 0.70	21.29 ± 1.00	22.17 ± 0.45
Na_2O	0.00 ± 0.00	0.49 ± 0.02	0.51 ± 0.03	0.44 ± 0.03	0.60 ± 0.15	0.76 ± 0.11
Total	99.99 ± 2.31	101.21 ± 1.83	100.27 ± 1.36	100.22 ± 2.37	100.32 ± 3.73	100.41 ± 2.12
Mg#	0.863 ± 0.005	0.841 ± 0.003	0.838 ± 0.005	0.847 ± 0.007	0.843 ± 0.018	0.824 ± 0.002

	AIN 25 (1) shonkinite	AIN 23 (7) malignite	AIN 23 (2) malignite	AIN 44 (5) malignite	AIN 44 (2) malignite	AIN 58 (3) rnalignite
SiO_2	53.26	53.13 ± 1.01	53.19 ± 0.64	52.74 ± 0.53	51.86 ± 0.05	52.10 ± 0.19
TiO_2	0.51	0.57 ± 0.16	0.73 ± 0.43	0.45 ± 0.08	0.78 ± 0.00	0.60 ± 0.09
Al_2O_3	2.08	1.23 ± 0.56	1.97 ± 1.41	1.27 ± 0.18	2.28 ± 0.09	1.51 ± 0.21
Cr_2O_3	0.05	0.03 ± 0.03	0.03 ± 0.01	0.23 ± 0.16	0.05 ± 0.01	0.03 ± 0.09
Fe_2O_3	4.38	8.41 ± 0.49	13.38 ± 0.61	2.99 ± 0.08	4.43 ± 0.06	5.93 ± 0.19
FeO	2.11	0.00 ± 0.00	0.00 ± 0.00	2.64 ± 0.48	2.76 ± 0.09	1.24 ± 0.83
MgO	15.75	14.93 ± 0.66	12.63 ± 0.55	16.19 ± 0.36	15.10 ± 0.08	15.68 ± 0.88
CaO	21.46	20.87 ± 0.84	16.43 ± 2.13	23.20 ± 0.14	22.34 ± 0.02	22.28 ± 0.23
Na_2O	0.85	1.68 ± 0.18	2.99 ± 0.23	0.58 ± 0.08	0.86 ± 0.06	1.15 ± 0.19
Total	100.45	100.85 ± 3.93	101.35 ± 6.01	100.29 ± 2.09	100.46 ± 0.46	100.51 ± 2.90
Mg#	0.823	0.778 ± 0.018	0.652 ± 0.002	0.844 ± 0.014	0.800 ± 0.003	0.809 ± 0.028

euhedral apatite, interstitial biotite with significant TiO_2-contents (4.3−5.7 wt.%), and subhedral magnetites with 3−8.5 wt.% TiO_2 (Table 3). The latter have exsolution lamellae of hercynite and ulvöspinel. Perthitic alkali feldspar (Or_{81-99}; Table 6) and minor feldspathoid are the main intercumulus phases. The K_2O-contents of the feldspathoids is about 20 wt.% (Table 7) and the Si/Al-ratio is ±2, which is indicative of leucite although it is generally not described from plutonic rocks. Nevertheless leucite was found in clinopyroxenites from the Batbjerg-complex in Greenland which are, together with jacupirangites, the main rock types at these locations (Brooks *et al.*, 1981).

Malignites. Malignites vary texturally from ortho- to noncumulates with 35 to 61 vol.% of intercumulus material. Clinopyroxene and biotite are the main cumulus phases that frequently appear as glomerophyric aggregates. Accessory phases are euhedral apatite and Ti-bearing magnetite. Rocks with more than 13.5 vol.% olivine in the cumulus assemblage are termed olivine-rich malignites, whereas those with only up to 4 vol.% olivine are named olivine-poor malignites (Table 1b). The dominant intercumulus phase is potassium feldspar with minor (pseudo)leucite and sodalite.

The olivine-rich malignites contain euhedral pale green clinopyroxenes which commonly encloses magnetite and/or apatite. Clinopyroxene analyses vary dominantly between $Ca_{42}Mg_{38}Fe_7$ and $Ca_{47}Mg_{47}Fe_{20}$ (Table 5). Olivine ($Fo_{>74}$) rarely has inclusions of magnetite. Subhedral magnetite is often mantled by unzoned TiO_2-rich (<5.8 wt.%) biotite. Potassium feldspar with Or_{67-94} and Ab_{3-20} is the dominant intercumulus phase (Table 6). A vermicular fingerprint intergrowth of potassium feldspar and sodalite is rarely found with cathodoluminescence.

Olivine-poor malignites are coarse grained with euhedral clinopyroxene and anhedral olivine (Fo_{45-74}). Both are extremely rich in inclusions of apatite, magnetite, and minor potassium feldspar. Clinopyroxenes enclose abundant needles of Fe-Ti-oxide often concentrated in zones parallel to the crystal faces. The clinopyroxenes characteristically have Na_2O >0.8 wt.% and are compositionally zoned. *Fs* increases outwards with a corresponding increase in Na suggesting an acmite component (Fig. 3e). Magnetites show anhedral shapes and are often mantled by biotite.

The intercumulus potassium feldspar with $Or_{90}-9_5$ and Ab_{5-15} is generally developed as patchy intergrowths of feldspar laths and minor feldspathoids (Table 7). Myrmekitic intergrowths with sodalite and fluorite is rarely found in interstices of the mafic cumulus minerals.

Mafic dyke rocks. The mafic dyke rocks were found only in drill cores. Although strongly altered, two petrographically different types can be recognized: (a) olivine-bearing rocks and (b) pseudoleucite-bearing rocks. Both have abundant pale green

TABLE 6. Representative energy-dispersive electron microscope analyses of feldspars from the Inagli rocks. AIN39 and AIN43 are olivine-rich malignites. AIN26 is an olivine-poor malignite; note the different FeOr content. The high TiO_2 values are likely to be due to Ba-Ti overlap in the EDS spectra. WDS analyses are not available to establish the Ba contents of the feldspars

	AIN 16 (14) shonkinite	AIN 25 (19) shonkinite	AIN 39 (8) ol-malignite	AIN 43 (10) ol-malignite	AIN 26 (10) malignite
SiO_2	65.38 ± 0.28	64.74 ± 0.30	63.71 ± 1.11	65.11 ± 0.11	66.07 ± 0.28
TiO_2	0.25 ± 0.08	0.88 ± 0.29	0.93 ± 0.68	0.35 ± 0.08	0.30 ± 0.14
Al_2O_3	18.97 ± 0.30	19.40 ± 0.36	20.11 ± 0.74	18.86 ± 0.17	18.32 ± 0.27
Fe_2O_3	0.00 ± 0.00	0.00 ± 0.00	0.00 ± 0.00	0.00 ± 0.00	0.18 ± 0.18
CaO	0.51 ± 0.20	0.48 ± 0.17	1.13 ± 0.47	0.50 ± 0.07	0.00 ± 0.00
Na_2O	0.82 ± 0.33	0.46 ± 0.37	1.38 ± 0.49	0.50 ± 0.13	1.06 ± 0.34
K_2O	14.05 ± 0.57	14.04 ± 0.78	12.76 ± 0.77	14.68 ± 0.17	14.08 ± 0.49
Total	99.98 ± 1.76	100.00 ± 2.27	100.02 ± 4.26	100.00 ± 0.73	100.01 ± 1.70
Mol.% end-member composition					
An	2.70 ± 1.06	2.69 ± 0.94	6.01 ± 2.51	2.65 ± 0.34	0.00 ± 0.00
Ab	7.90 ± 3.14	4.68 ± 3.76	13.09 ± 4.02	4.84 ± 1.23	10.29 ± 3.27
FeOr	0.00 ± 0.00	0.00 ± 0.00	0.00 ± 0.00	0.00 ± 0.00	0.66 ± 0.29
TiOr	0.31 ± 0.10	1.09 ± 0.44	1.19 ± 0.91	0.44 ± 0.11	0.37 ± 0.17
Or	89.00 ± 4.05	91.49 ± 4.37	79.71 ± 5.14	92.10 ± 1.34	88.68 ± 3.30
Total	99.91 ± 8.35	99.95 ± 9.51	100.00 ± 12.6	100.00 ± 3.02	100.01 ± 7.43

TABLE 7. Representative energy-dispersive electron microscope analyses of feldspathoids from the Inagli rocks. The analyses (normalized to 100%) represent, with two exceptions, leucite compositions and their calculation of structural formula, based on 6 oxygens. The analyses 26–38 and 43–45 represent a Na-rich feldspathoid. For TiO_2 contents: see Table 6 for caption

	16-47 shonk	16-118 shonk	25-28 shonk	25-33 shonk	26-38 malig	26-62 malig	39-23 malig	39-30 malig	39-43 malig	43-23 malig	43-45 malig
SiO_2	59.08	54.32	57.42	58.48	58.47	62.39	56.86	57.69	57.16	57.59	58.75
TiO_2	0.00	0.46	0.00	0.22	0.18	0.16	0.00	0.00	0.00	0.00	0.14
Al_2O_3	23.14	24.86	22.36	22.86	28.34	21.76	22.37	22.04	22.85	23.52	25.37
Fe_2O_3	0.26	3.23	0.00	0.00	0.00	0.00	0.00	0.00	0.23	0.00	0.00
CaO	2.60	2.12	0.13	1.01	0.00	0.48	0.40	0.00	0.22	1.02	2.12
Na_2O	2.69	3.60	0.00	2.15	12.18	4.93	0.00	0.00	0.49	1.76	9.03
K_2O	12.23	11.42	20.09	15.29	0.83	10.28	20.37	20.27	19.05	16.11	4.60
Total	100.00	100.00	100.00	100.00	100.00	100.00	100.00	100.00	100.00	100.00	100.00

Structural formula based on 6 oxygens

Si	2.054	1.918	2.059	2.056		2.135	2.047	2.069	2.044	2.035	
Ti	0.000	0.012	0.000	0.006		0.004	0.000	0.000	0.000	0.000	
Al	0.948	1.034	0.945	0.947		0.878	0.949	0.932	0.963	0.979	
Fe^{3+}	0.007	0.086	0.000	0.000		0.000	0.000	0.000	0.006	0.000	
Ca	0.097	0.080	0.005	0.038		0.018	0.015	0.000	0.008	0.039	
Na	0.181	0.246	0.000	0.147		0.327	0.000	0.000	0.034	0.121	
K	0.542	0.514	0.919	0.686		0.449	0.935	0.927	0.869	0.726	
Total	3.830	3.890	3.928	3.880		3.810	3.947	3.928	3.923	3.899	

clinopyroxenes. In the olivine-bearing rocks, olivine occurs as relicts and shows zoned alteration rims: the inner rim consists of iddingsite and the outer rim of clinopyroxene. Olivine and clinopyroxene occur in a microcrystalline groundmass rich in phlogopite, additional pyroxene, feldspar, as well as accessory spinel and apatite. The pseudoleucite-bearing rocks contain pseudoleucite phenocrysts which show a granular structure of secondary feldspar. The groundmass of these rocks is similar to the olivine-bearing rocks.

Isotopic data

K-Ar ages. Potassium-argon age determinations have been carried out on three clinopyroxenites, two shonkinites, two malignites and two phlogopite-rich veins crosscutting the dunites. The age data vary between 96 Ma and 146 Ma (Table 8).

No K-Ar dating was carried out on the dunites. Phlogopite concentrates from veins intersecting the dunites show little variation between 128.0 ±1.2 Ma and 131.6 ±1.3 Ma (Table 8). These values close to 131 Ma are interpreted as a minimum age for the dunites. The whole-rock ages of one olivine-clinopyroxenite are in the order of 122.3 ±1.2 and 125.1 ±1.2 Ma, whereas the corresponding

phlogopite yielded a distinctly younger age of 96.5 ±1.0 Ma (Table 8). Because of the low potassium content of the phlogopite, it seems that the age has been affected by alteration. From two phlogopite-clinopyroxenite samples, two phlogopite and whole rock fractions were analysed. Homogeneity problems were eliminated partly by double determinations of one fraction. The phlogopite data vary between 131.4 ±1.3 and 134.8 ±1.3 Ma (Table 8), and yielded a tightly constrained avarage of 132 Ma.

The determinations of two shonkinites resulted in a large variation of 96.9 ±1.0 to 118.7 ±1.1 Ma (Table 8). Similar to the phlogopite-clinopyroxenites, homogeneity problems were caused by the coarseness of these rocks as well as alteration. The whole-rock and potassium feldspar determinations of two olivine-poor malignites vary largely between 124.0 ±1.2 and 146.1 ±1.4 Ma (Table 8). In contrast, the biotite ages of 132.3 and 131.5 ±1.3 Ma (AIN 23) and 135.0 ±1.3 Ma (AIN 26) show only a small variation. These ages close to 133 Ma are in good agreement with one available biotite age of 129 ±5 Ma from a malignite (Kostyuk *et al.*, 1990).

Rb-Sr isotopes. Rubidium-strontium isotopic compositions were determined for mica, potassium feldspar and the whole-rock of one malignite. The

TABLE 8. K-Ar data of several grain size-fractions for the rocks from Inagli. The analytical error on the age is about 1%

Sample	Mineral	Size (μm)	% K	Vol^{40}Ar$_{rad}$ ccSTP/g10^{-6}	% ^{40}Ar	Age (Ma) ± error
phlog-dyke						
AIN 7	phlog	250−500	7.74	40.74	93.88	130.6 ± 1.3
	phlog	> 500	7.64	40.53	93.10	131.6 ± 1.3
AIN 27	phlog	250−500	8.48	44.65	97.84	130.6 ± 1.3
	phlog	> 500	8.40	43.40	95.83	128.2 ± 1.2
ol-cpx						
AIN 17	WR	125−200	0.227	1.116	79.27	122.3 ± 1.2
	WR	200−250	0.192	0.965	83.75	125.1 ± 1.2
	phlog	125−250	5.25	20.24	96.62	96.5 ± 1.0
phlog-cpx						
AIN 13	WR	125−200	2.05	9.70	97.40	117.7 ± 1.1
	WR	200−250	1.82	8.54	96.73	116.9 ± 1.1
	phlog	125−200	7.60	41.35	94.94	134.8 ± 1.3
	phlog	200−250	7.87	41.86	96.79	131.9 ± 1.3
AIN 14	WR	125−200	1.082	6.03	95.97	140.3 ± 1.4
	WR	200−250	0.877	5.126	96.94	144.4 ± 1.4
	phlog	125−200	8.07	43.04	98.17	132.2 ± 1.3
	phlog	200−250	8.28	43.82	98.48	131.4 ± 1.3
shonk.						
AIN 16	WR	60−80m	2.28	9.67	92.54	105.6 ± 1.0
	WR	80−100m	2.53	9.81	94.30	96.9 ± 1.0
AIN 25	WR	125−200	2.11	9.535	91.47	112.7 ± 1.1
	WR	200−250	2.06	8.819	89.14	106.9 ± 1.2
	k-fsp	125−200	11.26	49.69	91.72	110.1 ± 1.1
	k-fsp	200−250	11.28	53.81	98.69	118.7 ± 1.1
malig.						
AIN 23	WR	125−200	6.59	36.01	98.40	135.4 ± 1.3
	WR	200−250	6.44	34.42	98.29	132.5 ± 1.3
	bio	125−200	8.03	42.83	94.03	132.3 ± 1.3
	bio	200−250	7.61	40.35	94.77	131.5 ± 1.3
	k-fsp	125−200	11.07	55.24	98.82	124.0 ± 1.2
	k-fsp	200−250	10.88	55.74	98.70	127.2 ± 1.2
AIN 26	WR	125−200	5.20	30.46	96.95	144.7 ± 1.4
	WR	200−250	4.79	28.33	97.25	146.1 ± 1.4
	bio	125−250	7.12	38.80	95.04	135.0 ± 1.3
	k-fsp	125−200	10.73	62.20	97.37	143.3 ± 1.4
	k-fsp	200−250	10.67	61.32	97.13	142.1 ± 1.4

phlog – phlogopite; WR – whole rock; ol-cpx – olivine-clinopyroxenite; phlog-cpx – phlogopite-clinopyroxenite. For grain sizes AIN 16: m – mesh

results are presented in Table 9 and Fig. 4f. The intercept of the regression line gives a ^{87}Sr/^{86}Sr initial ratio of 0.70709 ± 0.00003. The corresponding model age of the isochron of 127.7 ± 1.1 Ma is about 5 Ma younger than the correponding biotite K-Ar ages of ± 132.3 Ma (Tables 8 and 9). This isochron provides a good contribution to the reliablity of the K-Ar age.

TABLE 9. Rb-Sr isotopic data of mineral and whole-rock fractions from one olivine-poor malignite from the Inagli-complex Analytical error is given as ± 0.0000xy or ± 0.000xyz

AIN23	Size (μm)	Rb ppm	Sr ppm	$^{87}Sr/^{86}Sr$ ± error	$^{87}Rb/^{86}Sr$ ± error
WR		190.0	1589.7	0.3458 ± 26	0.707672 ± 35
bio	125–200	406.3	31.8	37.165 ± 398	0.77453 ± 29
bio	200–250	378.8	152.2	7.207 ± 160	0.720281+49
K-fsp	125–200	262.9	1247.6	0.6102 ± 18	0.708259 ± 43
K-fsp	200–250	259.7	1237.7	0.6070 ± 18	0.708093 ± 57

bio – biotite; K-fsp – potassium feldspar; WR – whole rock

Discussion

The K-Ar data of ± 131 Ma of the phlogopite-rich veins cutting across the dunites indicate its minimum age. Similar ages of ± 132 Ma were obtained from phlogopites of phlogopite-clinopyroxenites. Biotites of the malignites vary at ± 133 Ma and correspond sufficiently to the Rb-Sr model age of 127.7 Ma. In summary, the data are interpreted to indicate the main period of generation and intrusion of the Inagli complex between 130 to 133 Ma which is in good accordance with the data by Kostyuk et al. (1990). The intrusion of the Inagli complex is thus more or less contemporaneous with the intrusion of other alkaline complexes in the Aldan-Shield (Mues, 1993; Mues-Schumacher et al., 1995).

Alternative models for the genesis of Inagli. Ultramafic rocks are known from ophiolites, alpine-type peridotites, stratiform intrusions and Alaskan complexes. Common peridotite minerals are olivine, (Al)-enstatite and (Al)-diopside with chromite-spinel and/or plagioclase or Cr-pyrope garnet. Al-spinel, Cr-spinel and chromites of lherzolites have Cr/(Cr+Al) ratios of <0.25, 0.25–0.65, and >0.65, respectively (Carswell, 1980). The Al_2O_3 contents are often up to 20 wt.% (e.g. Furnes et al., 1986). These mineralogical characteristics are distinctly different from those of the Inagli rocks which lack orthopyroxene and plagioclase, and the chromites of which have very low Al_2O_3 contents (<7%), resulting in very high Cr/(Cr+Al) ratios >0.8 (Fig. 3b). These differences rule out an origin similar to alpine-type peridotites.

Stratiform and layered intrusions such as, for example, the Bushveld or Skaergaard-complex generally show cyclic units often resulting in the generation of economically interesting ore deposits, e.g. chromitites (Stewart and DePaolo, 1990; Eales et al., 1990). Orthopyroxene and plagioclase commonly occur in the mineral assemblages of these rock series. Because the Inagli complex neither shows cyclic units documenting repeated replenishments of a magma reservoir, nor can orthopyroxene and plagioclase be recognized, thus emplacement history and chemistry of the Inagli parent magma(s) must be different from those of layered intrusions.

Alaskan-type complexes, as described by Ruckmick and Noble (1959), Taylor and Noble (1960, 1969), Irvine (1967, 1974), Taylor (1967), Findlay (1969), Murray (1972), and more recently by Brown et al. (1988), are generally relatively small intrusions that expose ultramafic rocks concentrically zoned around a central dunite body. Their compositional characteristics are distinctive: ideally, the cumulus rock series include dunite, wehrlitic peridotite, olivine clinopyroxenite, magnetite hornblende clinopyroxenite, and hornblende gabbro; orthopyroxene is sparse in these assemblages. Chromites with high Fe contents and very high Cr/(Cr+Al) ratios are diagnostic of Alaskan-type intrusions (Irvine, 1967, 1974). Most probably, parental magmas are a water-rich picritic ankaramite (Irvine, 1974) or an olivine-rich tholeiite (Murray, 1972). The Inagli complex shares many features with the Alaskan-type intrusions, such that a similar origin must be taken into account.

Mineral fractionation and parental magma composition. The lack of fresh volcanic rocks related to the plutonic rocks of Inagli and the ubiquitous evidence for cumulate textures obscure direct information about the composition of the parent magma(s). The following discussion, therefore, sets out to examine what can be inferred about the characteristics of the Inagli parental magma(s) and its differentiation history primarily based on petrographic observations, compatible element and *REE* systematics, and mineral data of the plutonic rocks precipitated from this liquid.

Shoshonitic affinity and tectonic setting. The ultramafic rocks, which predominate the Inagli complex, are characterized by a potassium affinity evidenced in the $K_2O – SiO_2$ diagram, where the rocks plot in the field for shoshonites (Fig. 4a). A
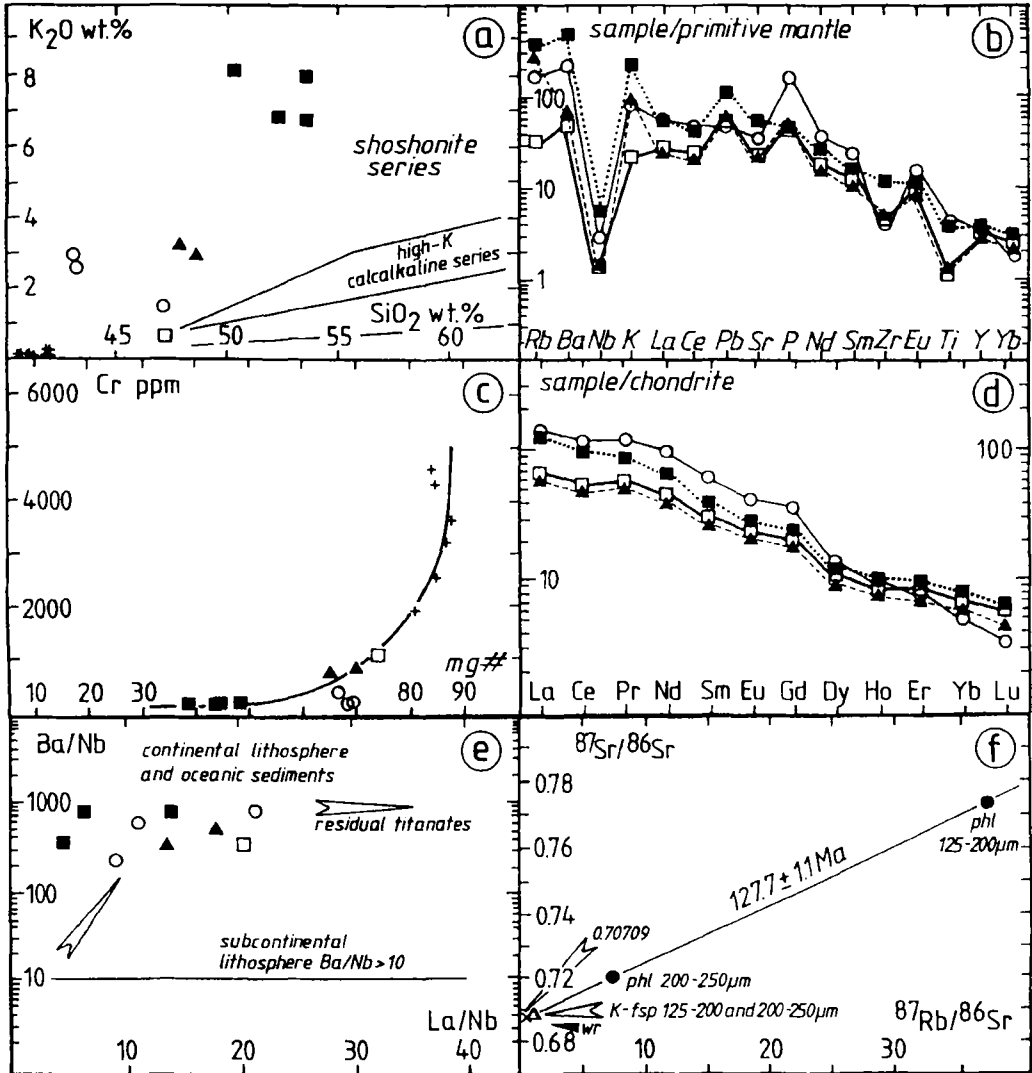
FIG. 4. Symbols as in Fig. 3. For detailed explanations see the text. (*a*) K_2O *vs.* SiO_2 variation diagram with the fields for shoshonite and high-K calcalkaline series for comparison. (*b*) Incompatible trace element distributions normalized to the primitive mantle of Sun and McDonough (1989) showing the overall similar patterns of all Inagli rocks. (*c*) Cr as a function of Mg# of the Inagli rocks shows a well constrained curved trend reflecting part of the fractionation history of the Inagli parental magma. (*d*) Chondrite-normalized *REE* patterns show the relative enrichment of the *LREE* over the *HREE*. (*e*) Ba/Nb *vs.* La/Nb ratios exemplify the *LILE/HFSE*- and *LREE/HFSE*-enrichments. (*f*) Diagram of the $^{87}Sr/^{86}Sr$ *vs.* $^{87}Rb/^{86}Sr$ ratios for the olivine-poor malignite sample AIN 23. The intercept of the regression line as an isochron with the $^{87}Sr/^{86}Sr$-axis gives the initial ratio.

shoshonitic affinity would also account for the relatively low Ti contents of clinopyroxene and phlogopite. The higher silica content of boninitic magmas with SiO_2 >53 wt.% and MgO >8 wt.% favours the crystallization of orthopyroxene. This is

reported, for example, from the Tasmanian ultramafic complexes with a predominance of olivine and orthopyroxene cumulates which are interpreted to represent high-level boninitic intrusions (Peck and Keays, 1990). Therefore, the high alkali and low

silica contents of the Inagli rocks would indicate a picritic primary melt rather than a boninitic one. The wide range in compatible elements such as Ni (2000–40 ppm) and Cr (4600–80 ppm; Fig. 4c) reflects the significant role of fractionation in the genesis of these rocks. Figure 4c, which features Cr as a function of Mg# reveals part of the fractionation history of the Inagli parental magma. In terms of these coordinates, ultramafic and mafic samples from Inagli define a well-constrained curved trend indicating sequential tapping of a fractionating system. We assume that the curvature of the trend for cumulate rocks represents the compositions of solids in equilibrium with liquids developing along a curved compositional trend.

Incompatible trace element distributions summarized in the primordial mantle-normalized spidergrams of Fig. 4b show almost identical patterns for all rocks. The enrichment in Low Field Strength Elements (LFSE) such as Ba, Rb and K, and the marked negative Nb anomaly are characteristics these rocks share with shoshonitic orogenic magmas (Pearce, 1982). Even if their K_2O/Na_2O ratios of 1.4–14.3 and $(La/Yb)_N$ ratios of 4–17 are higher and more variable than is common in shoshonitic magmas ($K_2O/Na_2O = 1$–0.7; $(La/Yb)_N = 8$–11), their general pattern compares favourably with those of shoshonitic series from active continental margins, particularly of those from, for example, the Mediteranean region (Ewart, 1982). The chondrite-normalized REE patterns of Fig. 4d show up to 200 times enrichment of the LREE La and Ce, and only 3 to 6 times chondritic values of the HREE Yb and Lu, resulting in $(Ce/Yb)_N$ ratios of about 11, indicating metasomatism by subduction-related fluids. Removal of olivine and chromite does not fractionate the REE, but merely increases their concentrations in the remaining liquid as simply documented by the different levels of enrichment.

The particular trace element systematics of the Inagli rocks are characterized by systematic high LILE/LREE and LILE/HFSE values, as shown by the pronounced low at Nb, relative lows at La and Ce (Fig. 4b) as well as by the high Ba/Nb and La/Nb ratios (Fig. 4e). These features require a LILE-rich component which is LREE- and HFSE-poor, to be responsible for the high LILE/LREE values, and a second component which is LILE- and LREE-rich and HFSE-poor. The first component, with its strong LILE enrichment over LREE is characteristic of low-K island arc tholeiites. Large ion lithophile element enrichment is widely attributed to hydrous fluids fluxing the mantle wedge from the subducting ocean crust (e.g. Jakes and Gill, 1970; Tatsumi et al., 1986). The second component with a similar degree of LREE and LILE enrichment is more typical of high-K arc basalts. The origins suggested for these basalts

are diverse and include incorporation of subducted sediments into the mantle wedge source and incompatible-element-enriched from subcontinental lithosphere (Eggins, 1993).

Sequence of crystallization. The Mg-numbers of olivines and pyroxenes provide a powerful tool for the identification of the differentiation stage of the melt they have crystallized from. Applied to the Inagli rocks, three groups are distinguished: (1) the dunites ($Fo_{>89}$) in the central part of the Inagli complex; (2) clinopyroxenites, shonkinites and olivine-rich malignites with Fo_{73-85} and $Mg\#_{px82-88}$; and (3) olivine-poor malignites ($Fo_{<70}$; $Mg\#_{px<82}$, px-core 1–2 wt.% Na_2O, px-rim up to 3.5 wt.% Na_2O).

With increasing amounts of clinopyroxene and feldspar, olivine abundances decrease and the rocks grade into clinopyroxenite, shonkinite, and malignite. The lithologies indicate early crystallization of olivine with minor chromite (Cr/(Cr+Al) >0.8) and phlogopite. The onset of clinopyroxene and minor apatite crystallization resulted in the formation of, for example, the olivine clinopyroxenites. This explains the high CaO contents of olivines (up to 0.55% CaO) in dunites contrasting with the lower CaO contents (<0.15%) in rocks with clinopyroxene (Table 2). This crystallization stage includes the olivine-clinopyroxenites (cpx 60%, ol 27%), shonkinites (cpx 48%, ol 20%) and olivine-rich malignites (cpx 35%, ol 15%) as the compositional Fe/Mg variation of the minerals is more or less the same. The olivine-poor malignites are interpreted to be late-stage highly evolved rocks whose olivines have low forsterite contents (Fo_{40-73}).

Thus, the crystallization sequence of the Inagli rocks can be tied to melt evolution using coexisting mineral compositions and Fe/Mg partitioning between olivine and 'basaltic' liquids (Fe/Mg_{Ol-liq} $K_D = 0.3$; Roeder and Emslie, 1970). Key reference points and associated melt Mg# values are:

(1) the most primitive phase is an olivine from a dunite as magnesian as Mg# 95.7 (melt Mg# 87.1).

(2) Cr-spinel formation accompanies crystallization of olivine less than approximately $Mg\#_{Ol} = 93.0$ (melt Mg# 80.1) that is indicated by Cr-spinel inclusions in olivines.

(3) Dunite formation persisted at least until olivine crystallization of Mg# 88.7 (melt Mg# 70.3).

The rarely observed interstitial phlogopites indicate either the beginning of phlogopite crystallization or the crystallization of phlogopite from trapped interstitial melt.

(4) Clinopyroxene (Mg# 87.1) begins crystallizing alongside olivine of Mg# 83.9 (melt Mg# 61.0), indicating that some of the olivines of the olivine-clinopyroxenites were formed before the onset of clinopyroxene crystallization.

Generally, olivine and clinopyroxenes are in equilibrium (based on expressions for Fe/Mg partitioning between both clinopyroxene and olivine and liquid (Barsdell, 1988; Roeder and Emslie, 1970) in olivine-clinopyroxenites.

(5) The onset of potassium feldspar crystallization during the formation of the olivine-clinopyroxenites cannot be linked to a maximum of Al content in clinopyroxene, as crystallization of phlogopite obscures this simple monitor.

(6) In some of the phlogopite-clinopyroxenites, shonkinites, and malignites, Fe/Mg partitioning between olivine and clinopyroxene indicate approximate equilibrium with only some few 'xenocrystal pyroxenes'. In others, the clinopyroxene has much too high Mg# for the corresponding olivine. This may either indicate 'xenocrystal' highly evolved olivine of high density, up to 3.85 g/cm^3 in these rocks, or ceased clinopyroxene crystallization and those found are 'xenocrystal'. The most fayalitic olivine of an olivine-poor malignite requires a melt composition as Mg-poor as a Mg#$_{liq}$ of 18.6. The Mg# disequilibrium relationships of olivine and clinopyroxene in these evolved rocks indicate that they do not come from one single differentiation stage of one liquid.

Properties of a potential parental melt. The parent melt composition of the Inagli complex must be as magnesian as Mg# 87.1. To model the MgO-contents required, a primitive picrite composition was chosen (Eggins, 1993). Model MgO contents were determined by adding small increments of equilibrium olivine to primitive liquid compositions until the olivine fractionation corrected bulk composition is in equilibrium with the most primitive olivine crystals. Following the procedure outlined above, MgO contents as high as 26.9 wt.% are required for the parent liquid of Inagli. This is quite high, nevertheless it seems reasonable, as lamproites from the Yakokut complex (about 40 km E of Inagli) have MgO contents of up to 25.7 wt.% (Mg# 83.9; Mg#$_{Ol}$ 94.0; Mues-Schumacher *et al.*, 1995). The above calculation using such a lamproite melt crystallizing an olivine of Mg# 95.7 results in an even higher MgO content of 28.2 wt.% from such a lamproitic parental melt.

Although the olivine of the dunite cumulate is of a highly refractory nature (Fo$_{95}$) requiring unusually high MgO-contents in the melt they have crystallized from, such Fo-rich olivines are reported from several different primitive arc basalts. Eggins (1993) compiled the most magnesian olivine phenocrysts found in primitive arc magmas including high-K alkaline basalts from Ambae (Vanuatu), and Oshima-Oshima (Japan) with up to Fo$_{94}$ for olivines as well as for clinopyroxenes. In this context, Inagli is clearly not the unusual occurrence of an anomalously high magnesian melt. Irrespective of whether picritic or

ultramafic primary melts are invoked, the high liquidus temperatures of such compositions ($\pm$1450°C at 2 GPa for picrites, and $\pm$1550°C at 3 GPa for ultramafic melts) require that melting takes place at anomalously high mantle temperatures (Eggins, 1992). However, these temperature values require the existence of a large thermal anomaly in the asthenospheric mantle beneath the Aldan Shield.

Conclusions

Field observations, petrographic, and chemical data were discussed in relation to: (a) the internal structure and formation of the potassium alkaline ultramafic cumulate series, and (b) properties of the parental liquid. Potassium-argon age determinations of phlogopites of $\pm$132 Ma give the age of the major period of formation of the Inagli complex.

The Inagli rocks represent different stages of the evolution of an ultrabasic liquid with continuous transitions of pure cumulate rocks to non-cumulus rocks. The high forsterite contents of the olivines indicate an ultrabasic parental melt such as an olivine-rich picritic melt. Calculations of the assumed MgO content of such a melt should be as high as $\pm$26 wt.% MgO. The general abundance of phlogopite demonstrates the presence of abundant water in the magma. The overall high *LILE* component and especially high potassium contents reflect the shoshonitic affinity of the parental Inagli magma. Characteristic high *LILE/LREE* and *LREE/ HFSE* ratios indicate a subduction zone component involved in the genesis of the Inagli rocks.

The overall geochemical signature of the ultramafic alkaline Inagli rocks, resembling potassic rocks from modern arcs, provides evidence that the Inagli intrusion could have formed in a similar tectonic environment. It may be that Inagli and other similar intrusions mark the change of geodynamic conditions from early Mesozoic arc-related compression (subduction zone component) to local extension (anomalous high temperatures due to upwelling of the convecting mantle).

analyses of the *REE* at Imperial College, London. Special thanks are also due to Peter Preschany, Wolfer & Goebel UTS, Stuttgart, who allowed UMS the use of all their office equipment.

References

Barsdell, M. (1988) Petrology and petrogenesis of clinopyroxenerich olivine tholeiitic lavas from Merelava Volcano, Vanuatu. *J. Petrol.*, **29**, 927–64.

Bilanenko, V.A., Spector, V.B. and Parfyonov, L.M. (1984) Geological outline of the Yakutsk ASSR. In: *Yakutsk ASSR–Siberian Platform, Guidebook of Geol. Conventus*, Moscow, 136–51.

Bilibin, J.A. (1961) *Late Jurassic Intrusions of the Central Aldan.* Moscow, 161 pp. (in Russian).

Brooks, C.K., Fawcett, J.J., Gittins, J. and Rucklidge, J.C. (1981) The Batbjerg complex, east Greenland: a unique ultrapotassic Caledonian intrusion. *Canad. J. Earth Sci.*, **18**, 274–85.

Brown, A.V., Page, N.J. and Love, A.H. (1988) Geology and Platinum-group-element geochemistry of the Serpentine Hill complex, Dundas Trough, Western Tasmania. *Canad. Mineral.*, **26**, 161–75.

Carswell, D.A. (1980) Mantle derived lherzolite nodules associated with kimberlite, carbonatite and basalt magmatism: a review. *Lithos*, **13**, 121–38.

Eales, H.V., De Klerk, W.J. and Teigler, B. (1990) Evidence for magma mixing processes within the Critical and Lower Zones of the northwestern Bushveld Complex, South Africa. *Chem. Geol.*, **88**, 261–78.

Edgar, A.D. (1987) The genesis of alkaline magmas with emphasis on their source regions: inferences from experimental studies. In: *Alkaline Igneous Rocks.* (J.G. Fitton and B.G.J. Upton, eds.) Geol. Soc. Spec. Publ., **30**, 29–52.

Eggins, S.M. (1992) Petrogenesis of Hawaiian tholeiites: 1, phase equilibria constraints. *Contrib. Mineral. Petrol.*, **110**, 387–97.

Eggins, S.M. (1993) Origin and differentiation of picritic arc magmas, Ambae (Aoba), Vanuatu. *Contrib. Mineral. Petrol.*, **114**, 79–100.

Eggler, D.H. (1978) The effect of CO_2 upon partial melting of peridotite in the system Na_2O-CaO-Al_2O_3-MgO-SiO_2-CO_2 to 35 kb, with an analysis of melting in a peridotite-H_2O-CO_2 system. *Amer. J. Sci.*, **278**, 305–45.

Ewart, A. (1982) The mineralogy and petrology of Tertiary-Recent orogenic volcanic rocks: with special reference to the andesitic-basaltic compositional range. In: *Andesites: Orogenic Andesites and Related Rocks.* (R.S. Thorpe, ed.) John Wiley, New York. pp. 25–95.

Findlay, D.C. (1969) Origin of the Tulameen ultramafic-gabbro complex, southern British Columbia. *Canad. J. Earth Sci.*, **6**, 399–425.

Flisch, M. (1986) K-Ar-dating of quaternary samples. In: *Dating Young Sediments* (A. Hurford, E. Jager and J.A.M. Ten Cate, eds.), CCOP technical secretariat, Bankok, Thailand, 299–323.

Furnes, H., Pedersen, R.B. and Maaloe, S. (1986) Petrology and geochemistry of spinel peridotite nodules and host basalt, Vestspitsbergen. *Norsk Geol. Tids.*, **66**, 53–68.

Hurford, A., Jäger, E. and Ten Cate, J.A.M. (1986) *Dating Young Sediments.* CCOP technical secretariat, Bankok, Thailand.

Irvine, T.N. (1967) The Duke Island ultramafic complex, southeastern Alaska. In: *Ultramafic and Related Rocks.* (P.J. Wyllie. ed.), Wiley & Sons, New York, 84–97.

Irvine, T.N. (1974) Bridget Cove volcanics, Juneau area, Alaska: possible parental magma of Alaskan-type ultramafic complexes. *Car. Inst. Geophys. Lab.*, **72**, 478–91.

Jakes, P. and Gill, J. (1970) Rare earth elements and the island arc tholeiite series. *Earth Planet. Sci. Lett.*, **9**, 17–28.

Kortschagin, A.M. (1972) Inagli-massive of ultrabasic and alkaline rocks (southern Yakutia). *1st. AN SSSR, ser. geol.*, **7**, 49–59 (in Russian).

Kortschagin, A.N. (1986) The metasomatites of Inagli. *Geol.ser. UDK*, **552**, 46–54 (in Russian).

Kostyuk, V.P. (1983) The potassic alkalic magmatism of the Baikal Aldan Belt. *Sov. Geol. Geophys.*, **24**, 31–8 (in Russian).

Kostyuk, V.P., Panina, L.I., Zhidkov, A.Ja., Orlova, M.P. and Bazarova, T.Ju. (1990) Potassic alkaline magmatism of the Baikal-Stanovoy rift system. *Novosib. Nauka*, **239** (in Russian).

LeBas, N.J., LeMaitre, R.W., Streckeisen, A. and Zanettin, B. (1986) A chemical classification of volcanic rocks based on the TAS-diagram. *J. Petrol.*, **27**, 745–50.

LeMaitre, R.W. *et al.* (1989) *A classification of igneous rocks and glossary of terms.* IUGS (R.W. LeMaitre, ed.) p. 128.

Maksimov, E.P. (1972) Ring-type magmatic complexes of the Aldan-Shield. *1st. AN SSSR, ser. geol.*, **3**, 33–44 (in Russian).

Mitchell, R.H. and Bergman, S.C. (1991) *Petrology of Lamproites.* Plenum Press, New York. p. 447.

Mues, U. (1993) *Geochemische und radiometrische Untersuchungen an Lamproiten und anderen Alkaligesteinen von Yakokut und Inagli, Aldan-Schild, Ostsibirien.* PhD thesis Univ. Freiburg, pp. 158.

Mues-Schumacher, U., Keller, J., Kononova, V.A. and Suddaby, P. (1995) Petrology and age determinations of the ultramafic (lamproitic) rocks from the Yakokut complex, Aldan Shield, Eastern Siberia. *Mineral. Mag.*, **59**, 409–28.

Murray, C.G. (1972) Zoned ultramafic complexes of the

Alaskan-type: feeder pipes of andesitic volcanoes. *Geol. Soc. Amer.*, **132**, 313–35.

Pearce, J.A. (1982) Trace element characteristics of lavas from destructive plate boundaries. In: *Andesites: Orogenic Andesites and Related Rocks.* (R.S. Thorpe, ed), 525–48.

Peck, D.C. and Keays, R.R. (1990) Geology, geochemistry, and origin of Platinum-group element-chromitite occurrences in the Heazlewood river complex, Tasmania. *Econ. Geol.*, **85**, 765–93.

Perchuk, L.L., Aranivich, L.Ya., Podlesskiy, K.K., Lavrant'eva, I.L., Gerasimov, V.Yu., Fed'kin, V.V., Kitsul, V.I., Karsakov, L.P. and Berdnikov, N.V. (1985) Precambrian granulites of the Aldan-Shield, eastern Siberia. *J. Metamorph. Geol.*, **3**, 265–310.

Roeder, P.L. and Emslie, R.F. (1970) Olivine-liquid equilibrium. *Contrib. Mineral. Petrol.*, **29**, 275–89.

Ruckmick, J.C. and Noble, J.A. (1959) Origin of the ultramafic complex at Union Bay, southeastern Alaska. *Geol. Soc. Amer. Bull.*, **70**, 981–1018.

Steiger, R.H. and Jäger, E. (1977) Subcommission on geochronology: convention on the use of decay constants in geo- and cosmochronology. *Earth Planet. Sci. Lett.*, **36**, 359–62.

Stewart, B.W. and DePaolo, D.J. (1990) Studies of processes in mafic magma chambers: II. The Skaergaard intrusion, East Greenland. *Contrib.*

Mineral. Petrol., **104**, 125–41.

Sun, S.S. and McDonough, W.F. (1989) Chemical and isotopic systematics of oceanic basalts: implications for mantle composition and processes. In: *Magmatism in Ocean Basins* (A.D. Saunders and N.J. Norry, eds.) Geol. Soc. Spec. Publ., **42**, 313–45.

Taylor, H.P., Jr. (1967) The zoned ultramafic complexes of southeastern Alaska. In: *Ultramafic and related rocks.* (P.J. Wyllie, ed.) Wiley & Sons, New York, 97–121.

Taylor, H.P., Jr. and Noble, J.A. (1960) Origin of the ultramafic complexes in southeastern Alaska. *Int. Geol. Cong.*, 21st, Copenhagen, Comptes Rendus Sec. **13**, 175–87.

Taylor, H.P., Jr. and Noble, J.A. (1969) Origin of magnetite in the zoned ultramafic complexes in southeastern Alaska. In: *Magmatic Ore Deposits.* (H.D.B. Wilson, ed.) Econ. Geol. Mon., **4**, 209–30.

Tatsumi, Y., Hamilton, D.L. and Nesbitt, R.W. (1986) Chemical characteristics of fluid phase released from a subducted lithosphere and origin of arc magmas: evidence from high-pressure experiments and natural rocks. *J. Volcanol. Geotherm. Res.*, **29**, 293–309.

Wyllie, P.J. (1978) Peridotite-CO_2-H_2O and the Low-Velocity Zone. *Bull. Volcanol.*, **41**, 670–83.